Shock waves in materials with Dzugutov-potential interactions

Johannes Roth
Institut für Theoretische und Angewandte Physik, Universität Stuttgart, Pfaffenwaldring 57, 70550 Stuttgart, Germany
(Received 15 June 2004; revised manuscript received 31 May 2005; published 26 July 2005)

The influence of shock waves on the bcc ground state, the metastable σ phase, and quasicrystal structures of the Dzugutov potential [Phys. Rev. A **46**, R2984 (1992)] has been studied by molecular dynamics. In general, a phase transition is observed to the well-known high-pressure fcc- or hcp-phase. The details of the phase transition and the perfection of the created phases depend on the orientation of the shock wave propagation direction with respect to the symmetry axes. The results are in good qualitative agreement with recent simulations with embedded atom method potentials designed specifically for iron. For the quasicrystal we observed flips, a new plasticity mode predicted for these structures. Furthermore we will report the results for an amorphous structure supplied with the same potential. No crystallization takes place in this case, indicating that it is easier to shift atomic layers collectively than to order the atoms one by one.

DOI: 10.1103/PhysRevB.72.014125 PACS number(s): 62.50.+p, 61.44.Br, 02.70.Ns

I. INTRODUCTION

Shock wave experiments and simulations are useful tools to expose a solid-to-strong uniaxial stress and to study plasticity induced by defects or phase transitions without prior assumptions about the possible mechanisms. The action of shock waves has been explored in monatomic crystals to some depth,[1,2] and a first understanding of the basic processes has emerged.[3] The generation of partial dislocations and stacking fault type defects in fcc crystals could be clarified.[4] Results for the plasticity of other structures, such as bcc iron for example, are also available now.[5]

The purpose of the present study is to find out whether monatomic quasicrystals behave differently than crystalline materials if they are penetrated by shock waves. Most naturally occurring quasicrystals are ternary alloys. Stable binary quasicrystals have been discovered only very recently.[6] Shock waves in binary quasicrystals have been studied, and it was found that the results for quasicrystals and crystals depend primarily on the atomic interaction and not on the structure.[7]

From a fundamental point of view it is more interesting, however, to study models as simply as possible, i.e., monatomic quasicrystals. But the number of such models is rather limited if generic interactions are favored. The crucial point is the packing density. There is the unit sphere packing model of Henley[8] with a density of 0.6288, still worse than the random close packing at 0.6366. Treated as a quasicrystal with Lennard-Jones interactions, the structure is metastable only up to 10% of the melting temperature of the ground-state fcc crystal.[9,10] It is the only promising monatomic icosahedral quasicrystal model known to us. Henley's twelvefold site model[8] has a much lower packing density and so is even less stable. Other models are layered quasicrystalline, which are periodic in one direction. The decagonal model of Cockayne and Mihalkovič[11] has a packing density of 0.6953, higher than the icosahedral model and larger even than bcc. But it also transforms into fcc upon heating if the atoms interact via Lennard-Jones potentials. Finally there is a dodecagonal quasicrystal model with Dzugutov-potential interactions. Its phase diagram has been studied in detail.[12,13] Although Dzugutov[14] has obtained a quasicrystal by cooling a melt, it is not a ground state for this interaction at zero temperature. Another crystal structure, namely the σ phase, which may be regarded as a low-order quasicrystal approximant, is more stable than the quasicrystal. But even more stable and the true ground state at zero temperature is a bcc crystal. The stable structures at high pressure and low temperature are even close-packed fcc phases or hcp phases. Upon heating at low pressure, bcc, the σ phase, and the quasicrystal phases are stable up to rather similar melting temperatures. This is the reason why shock-wave simulations have been carried out with these structure models and the Dzugutov potential.

The work is being described in two papers. Here we present the results of shock wave simulations in the different structures stable with Dzugutov interactions. In a second paper[15] (called paper II in the following) we concentrate on the phenomenon of solitary waves observed especially in the bcc structure shocked along the threefold axis and discuss in detail the hexagonal ω phase,[16] a typical product of a bcc lattice instability. The present paper is organized as follows. We first describe the simulation setup and the structure models. The next sections contain the results for each of the models and for the different orientations, followed by a short account of the soliton phenomenon. A thorough discussion of the latter will be given in the second paper. We close with a discussion of the results.

II. GENERATION OF THE SHOCK WAVES AND SIMULATION SETUP

A. The structures

Shock waves have been generated in three-dimensional dodecagonal quasicrystals, in the Frank-Kasper-type σ phase and in bcc crystals. The bcc structure may be regarded as a tetrahedrally close-packed (tcp) phase and therefore has some similarity to the Frank-Kasper phases. From this point of view, bcc contains disclinations where six tetrahedra meet along a common edge and antidisclinations where four tetrahedra meet, whereas ordinary Frank-Kasper phases contain

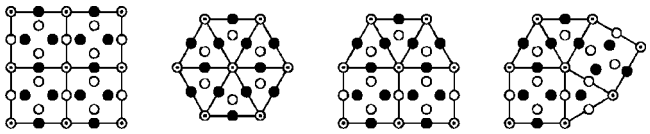

FIG. 1. Possible vertex configurations in square-triangle tcp phases. From left to right: A phase, Z phase, H phase, and σ phase.

disclinations only. The σ phase is such an ordinary Frank-Kasper phase with squares and triangles as basic motives. The σ phase and other related phases together with dodecagonal quasicrystals have been described in detail by Roth.[12] Here we will recollect only the most important aspects of the structure.

The unit cell of the σ phase can be subdivided into building blocks that look like two regular triangles and two squares if projected onto the basis plane perpendicular to the fourfold direction (Fig. 1). The building blocks will be called tiles in the following and we will simply speak of squares and triangles. Two squares and three triangles meet at each vertex in such a way that the squares have no common edge. The arrangement of the atoms can be read off from Fig. 1. The vertices of the squares and triangles are decorated with atoms at $z=0$ and $z=\frac{1}{2}$ (dotted circles). These are the basic A layers. The edge centers of the squares are alternatively decorated at $z=\frac{1}{4}$ and $z=\frac{3}{4}$ (filled and empty circles). The interior of the squares contains four additional atoms. Atoms nearest to each other in projection are placed in different layers. The atoms at the edge centers of the triangles are all either at $z=\frac{1}{4}$ or at $z=\frac{3}{4}$, the interior atom is again in the layer not occupied by the edge atoms. The atoms at $z=\frac{1}{4}$ and $z=\frac{3}{4}$ form the B and $\bar{B}$ layers, respectively, locally equivalent up to translations and rotations. The atoms at the vertices of the tiles are 14-fold coordinated, while the atom in the center of the triangles is 15-fold coordinated. The remaining atoms on the edges and in the interior of the square are 12-fold coordinated nonregular icosahedra. Since all coordination shells have a triangular surface, all atoms are tetrahedrally close packed.

Other combinations of squares and triangles are also possible. There are three additional phases in which all vertices are of the same type.[19] They are presented in Fig. 1. These phases are less stable than the σ phase, so they will not be considered further in this paper. If more than one vertex type is allowed, the number of possible phases grows very rapidly, even for crystalline structures.[20]

The quasicrystal is built of the same square and triangle tiles. We have studied random tilings only in this paper although it is possible to construct perfect quasicrystals with the help of matching rules or by inflation. In the quasicrystal model, the tiles of the primary layer are arranged in such a way that the structure has dodecagonal symmetry on average. The B and $\bar{B}$ layers have hexagonal symmetry only. They are mapped onto one another by the 12-fold symmetry. It is possible to introduce additional tiles, for example the hexagons (see Fig. 2), and to construct more general quasicrystalline structures, but they will not be considered here since these configurations are not as stable as the pure square-triangle tiling.

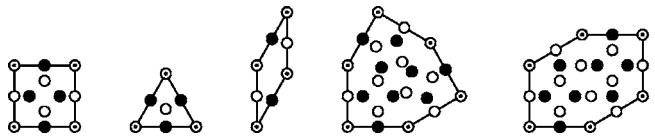

FIG. 2. Primary and additional tiles observed in the square-triangle tcp phases. From left to right: square, triangle, rhombus, threefold, and twofold symmetric hexagon.

Additional tiles are found in crystalline samples already (see Fig. 2). Especially rhombi may occur as localized defects or represent grain boundaries. The rhombi are not stable if they occur in pairs or larger aggregates. The two hexagons have not been observed in crystals. They may be viewed as transition states that can split into the other tiles.

Figure 3 represents a special approximant of a quasicrystal, which has been chosen such that most of the tiles and vertex configurations are present.

B. Orientation of the samples

For the simulation of shock waves it is necessary to apply periodic-boundary conditions. Otherwise the pressure from the shock wave leads to rapid transverse disintegration. The direction of the shock wave has to be parallel to one of the boundary axes, for example, the x axis. This limits the possible (quasi-)crystalline directions along which the shock wave can travel in the simulations. The quasicrystal, especially, has to be replaced by an orthorhombic approximant. Shock waves have been studied in the bcc phase along the fourfold, threefold, and twofold axes where they are straightforward to implement. Shock waves in the square-triangle quasicrystal have been studied along the periodic axis and in the quasiperiodic plane. Due to the high 12-fold symmetry (space group $12_6/mnm$) the quasicrystal is expected to be elastically isotropic in the plane, and the approximant should

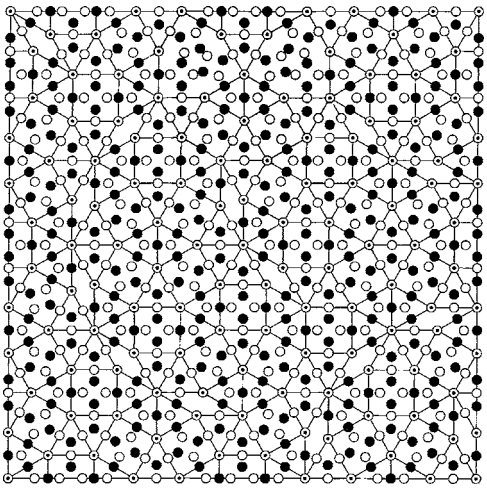

FIG. 3. Part of a dodecagonal quasicrystal. The atoms in the basic A layers $z=0$ and $z=\frac{1}{2}$ are dotted. The black atoms are in the B layer at $z=\frac{1}{4}$, the white atoms are in the $\bar{B}$ layer at $z=\frac{3}{4}$. The edge length is usually of the order of $2a$, the nearest-neighbor distance, but depends on the interaction between the atoms.

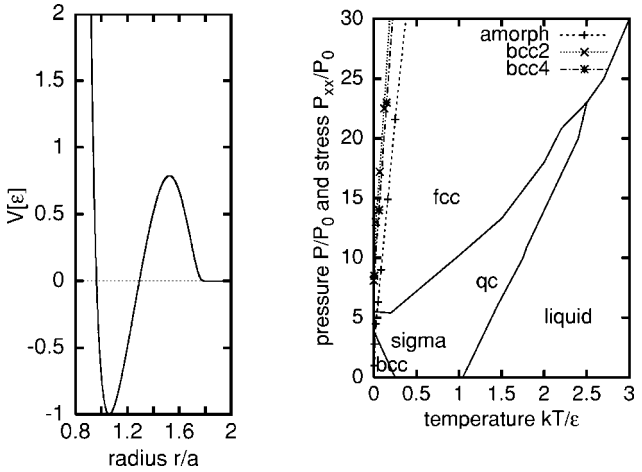

FIG. 4. Left: The Dzugutov potential in the parametrization applied in this work. Right: Semiquantitative phase diagram of the Dzugutov potential. The stress-temperature curves for shocked states are presented for materials initially amorphous (Sec. III C 5) and bcc shocked along the twofold and fourfold axes (Sec. III). The curves for other initial structures and directions are similar to bcc.

not deviate too much from isotropy. Shock waves along different in-plane directions should therefore give similar results. The σ phase has space-group symmetry $4_2/mnm$, which means that for an ordinary, nearly cubic unit cell with 60 atoms the coordinate axes are parallel to the fourfold axis and to glide planes n, and the diagonals are parallel to mirror planes m. A diagonal tetragonal unit cell with 30 atoms is also possible with the fourfold axis and the m planes parallel to the coordinate axes. The aspect ratio of these two unit cell lengths in the plane and along the z direction is such that it is possible to construct "diagonal" cubic boxes with only minor distortion of the structure and to rotate them by 45°. In summary we have studied shock waves in the σ phase along the fourfold axis, along the n and m directions, and along orientations at 45° between the fourfold direction and n and m, respectively. The directions will be denoted by 0, $n90$, $m90$, $n45$, and $m45$. The corresponding Miller indices are [100], [001], [011], [201], and $[\sqrt{8}11]$.

C. The Dzugutov potential and phase diagram

Reduced units are used throughout the paper. Lengths are given in a and energies in ϵ. All other units are converted into a, ϵ, and the mass m. Thus we have $t_0 = a\sqrt{m/\epsilon}$, $v_0 = \sqrt{\epsilon/m}$, and $P_0 = \epsilon/a^3$.

Dzugutov has invented his potential[17] to study the glass transition of monatomic liquids. It turns out that the potential has a number of interesting properties, especially stabilizing monatomic dodecagonal quasicrystals. It is similar to the Lennard-Jones potential from the core down to the minimum at $r = 1.061a$ and $V = -1\epsilon$, a being the interatomic distance (see Fig. 4, left). The minimum is followed by a maximum at $r = 1.5282a$ and $V = 0.7906\epsilon$, designed to disfavor square arrangements of nearest-neighbor atoms prominent in close-packed crystal structures at ambient pressure. The potential has a built-in cutoff radius of $r_c = 1.805a$. If the density of the structure is increased, the interatomic distances shift and the close-packed structures becomes more favorable than bcc and the σ phase.

The phase diagram of the Dzugutov potential has been determined by means of molecular dynamics simulations and thermodynamic perturbation theory[12] and improved recently by direct free energy calculations at low temperatures[18] (see Fig. 4, right). It turns out that the bcc phase is the ground state only in a very small triangular pocket between $kT = 0$, $P = 0$; $kT = 0.4\epsilon$, $P = 0$; and $kT = 0$, $P = 5.5P_0$, but is metastable in the whole range of stability of the σ and quasicrystal phases. Close-packed phases with different stacking sequences are largely degenerate due to the short-range nature of the potential, which ranges only up to the third neighbor shell. These phases are stable above about $P = 6P_0$. The phase boundary moves slowly to higher pressures with increasing temperature and reaches $P = 10P_0$ at $kT = 1\epsilon$ ($kT = 1.02\epsilon$ is the melting temperature of the σ phase and the bcc phase at $P = 0$). The σ phase seems to be the stable phase below $P = 6P_0$ and above the domain of the bcc phase. Care must be taken here, however, since with increasing temperature other tcp phases and especially the quasicrystal phase may become more stable than the σ phase due to the additional entropy caused by the freedom to (re)arrange the tiles. The location in the phase diagram where the quasicrystal phase has been discovered is indeed included in the stability domain of the σ phase.[14]

D. Sample size and preparation

All simulations have been carried out with the IMD which means ITAP Molecular Dynamics simulation package.[24] The sizes of the samples depend on the structures and orientations. Therefore they will not be listed in detail. For most of the simulations the sample size was about $(20 \times 20 \times 100)a^3$. The samples contained about 40 000 atoms. To study the influence of the size of the samples and the propagation time of the shock wave on the results longer ($200a, 300a$, and $600a$ long with up to 250 000 atoms) and thicker samples [$(40 \times 40 \times 300)a^3$ with 500 000 atoms] have also been analyzed. The principal results are found to be independent of the sample sizes. There were minor differences in the details, but there were no differences, for example, in the shock wave propagation velocities or in the phase transitions.

Equilibrations were performed with the number density × velocity × time (nvt) Nosé-Hoover and N-P-T Andersen ensemble. At low temperature and pressure the differences between nvt and N-P-T equilibration are marginal. Before the simulation starts, the samples are equilibrated for a time interval of $\Delta t = 10t_0$ at a temperature of $kT = 0.001\epsilon$ and a pressure of $P = 0.01P_0$. If the simulations are carried out at elevated temperatures, the samples are equilibrated again at the desired temperature. If necessary, the samples are quenched to $kT = 0.0$ after simulation to simplify the analysis of the results.

For the shock simulations a constant number of molecules, volume, and energy (NVE) ensemble was used. There are a number of well-established methods to generate shock

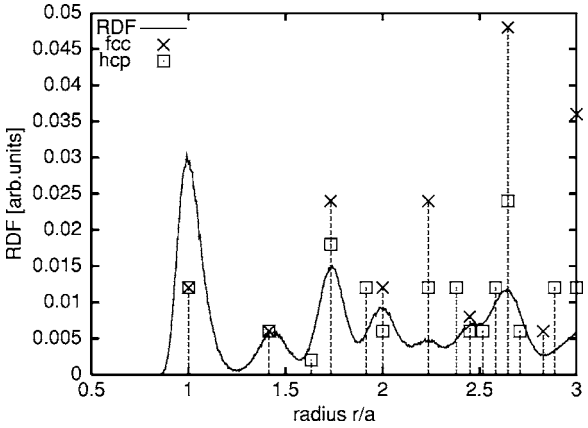

FIG. 5. Typical radial distribution function. The spikes indicate the neighbor shells for ideal fcc (×) and hcp (□) crystals. Obviously, these cases cannot be distinguished in the simulation result.

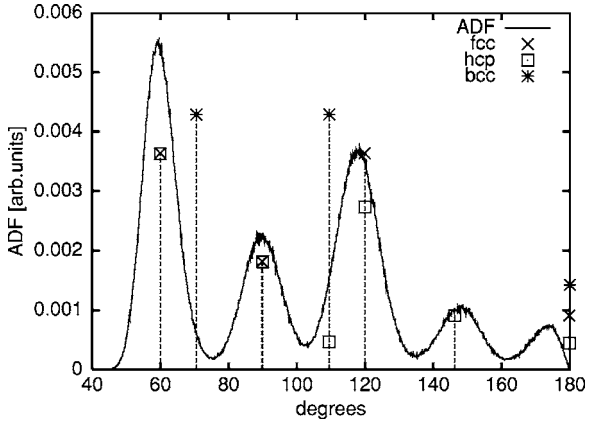

FIG. 6. Typical angular distribution function. The spikes denote the angles in ideal fcc (×), hcp (□), and bcc (*), respectively. The simulation result does not fit to the bcc maxima, but to fcc or hcp. A distinction between the latter is possible since the maximum between 140° and 160° is only present in hcp. The conclusion is that the sample under consideration is preferably hcp stacked. Cases without a maximum between 140° and 160° have also been observed.

waves in simulations.[3,21] In the present work we have applied the momentum mirror method: As soon as the atoms reach the upper end of the sample, their velocities are inverted. Thus the atoms behave as if a second sample is colliding with the simulated one. Tests have shown that the results for the mirror method are equivalent to the simulation with the collision method. Consequently the boundary conditions are periodic only in transverse direction whereas open boundaries exist at the end of the sample opposite to the mirror.

E. Analysis tools for the shocked structures

If the shocked state is monocrystalline as for bcc shocked along the fourfold direction at low piston velocities, then the analysis can be carried out directly by visual inspection of the structures. The stacking sequence can be derived from a projection of the atoms perpendicular to the distinguished threefold axis: A zigzag pattern determines hcp; a diagonal sequence determines fcc. In general we find a mixture of both.

Usually the shocked crystals are very defective, the lattice rows and planes are warped and rotated, twins or several crystallites may exist. A direct distinction between fcc or hcp or more complicated stackings is no longer possible. The radial distribution function (RDF) tells us only that a close-packed phase has been generated (Fig. 5).

But if the angular distribution function (ADF) is computed for nearest-neighbor atoms only, then it is possible to distinguish fcc and hcp (Fig. 6) since hcp permits an additional maximum between 140° and 160° (the angle between the apex atoms and a base atom of two face-connected tetrahedra). In most cases a mixture of fcc, hcp, and other stacking sequences is found.

We have tried to quantify the fraction of fcc and hcp using the common neighbor analysis.[22,23] The first difference between fcc and hcp occurs for the 1421 and 1422 diagrams. In fcc crystals there are no 1422 diagrams whereas the fraction of 1421 and 1422 diagrams should be equal for hcp. There is a problem, however: In amorphous structures, the 1422 are twice as frequent as the 1421. Thus it is not possible to distinguish fcc and hcp quantitatively by the 1421 and 1422 diagrams if substantial disorder is present. The inclusion of other diagrams into the analysis such as 1555, 1544, and 1433 for icosahedral order or the most frequent second-neighbor diagrams 2333, 2211, and 2100 did not help to resolve the ambiguities.

III. RESULTS

The stress-temperature behavior of the shocked material is included in the equilibrium phase diagram (Fig. 4). The curves are rather similar for all initial structures as far as a unique temperature can be defined. This is not the case within the transition region from unshocked to shocked where the initial structure is destroyed in several steps and the final structure has to be formed. For details see Sec. III C. Thus we do not find a thin shock front to which we could apply the standard jump conditions. The stresses and temperatures have been determined directly from the simulation results of the shocked state. The stress-temperature curves are always very steep and do not cross the melting line up to very high pressures ($P > 180P_0$).

In the following sections we will present the results of the shock wave simulations in detail. We will start with the elastic properties of the materials since they form the limiting case of very weak shock waves where the strength of the material prohibits the creation of defects. The next step is the discussion of the relation between the piston velocity u_p and the speed of the shock wave u_s represented in a Hugoniot diagram. In the mirror method setup the shock velocity is obtained from the velocity of the sample u_p and the shock propagation velocity v observed in the laboratory reference frame by $u_s = v + (-u_p)$. The Hugoniot diagram permits a classification and characterization of different shock wave regimes. The following is a presentation of the phase transfor-

TABLE I. Elastic properties for the bcc phase. The first column gives the Miller indices, the second the uniaxial elastic modulus, and the third the velocity of the quasilongitudinal wave. The bcc crystals are obviously anisotropic.

Direction	$F[P_0/m]$	$c[v_0]$
[100]	287.0	16.6
[110]	387.0	19.3
[112]	389.4	19.4
[111]	424.8	20.2

mation results grouped together with respect to similar phenomena.

A. Elastic properties and sound velocities

Dodecagonal quasicrystals behave elastically isotropic with respect to the quasicrystalline plane, but not with respect to the periodic axis, similar to hexagonal crystals. The σ phase is anisotropic in the square-triangle plane since it has only tetragonal symmetry. The bcc crystals have cubic symmetry. The elastic constants determined by quasistatic uniaxial deformations are presented in Tables I and II. If the piston wave velocity u_p goes to zero, the shock wave velocity tends toward the velocity of an elastic sound wave.

It is important to note that the highest velocities of sound occur along directions perpendicular to the thinnest crystal planes, or equivalently, parallel to the densest atomic rows. These are the directions where the solitary waves (see Paper II) are most prominent.

B. The Hugoniot relation: u_s versus u_p and wave profiles

In the case of shock waves in two-atomic Laves crystals and quasicrystals,[6] three regimes of different behavior of the shocked materials have been observed. The same is true here, although at a first glance the Hugoniot diagram (Fig. 7) looks different: There seem to be only two ranges, separated at about $u_p=0.25c_x$, if c_x is the uniaxial velocity of sound of structure x.

TABLE II. Elastic properties of the tcp phases. The first column gives the Miller indices; the second and fourth, the uniaxial elastic modulus; and the third and fifth, the velocity of the quasilongitudinal wave for quasicrystals and the σ phase, respectively. The first three rows contain the results for the perfect samples; the last two rows list the results for samples that have been distorted to permit periodic boundary conditions parallel to the 45° direction. A comparison of the second and third rows and the fourth and fifth rows, respectively, shows that the quasicrystal is isotropic within the error margins whereas the σ phase possesses a moderate anisotropy of the order of 6%.

	Quasicrystal		σ Phase	
Direction	$F[P_0/m]$	$c[v_0]$	$F[P_0/m]$	$c[v_0]$
[100]	298.4	16.8	299.2	16.8
[010]	179.2	13.0	180.4	13.1
[011]	177.0	13.0	203.0	13.9
[201]	216.8	14.3	248.0	15.4
$[\sqrt{8}11]$	200.6	13.8	208.2	14.0

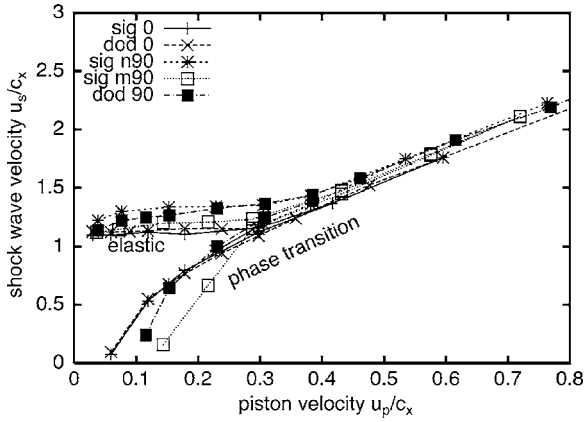

FIG. 7. Hugoniot diagram for σ phase and quasicrystal simulations. The axes are scaled with the velocities of sound. The lines serve as a guide to the eye only. The two parallel branches indicate the beginning and end of the phase transformation.

The reason is that the elastic first range is very small since the transition from bcc and σ phase to close packed takes place at about $P=5.5-6P_0$, and this pressure is reached at $0.03-0.05c_x$. Furthermore no retardation effect is observed. The elastic wave velocity is difficult to determine since no sharp wave fronts exist. Therefore it is not included in the diagram.

In the range between $u_p=0.05$ and about $0.2-0.25c_x$ we observe steady and unsteady wave fronts, depending on the orientation of the samples and the character of the phase transition. In this range the shock speed of the uniaxial compression wave is more or less constant whereas the velocity of the slower transformation wave grows rapidly (Figs. 7 and 8). It is remarkable that the two wave fronts taken separately are steady although relaxation and healing of defects occurs for the second. The wave profile as a whole is not steady since the different wave fronts have different velocities.

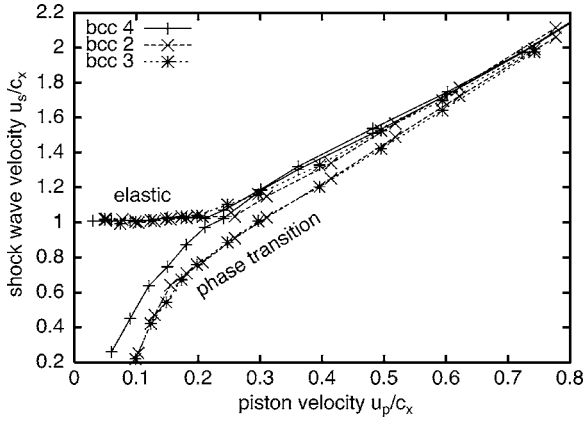

FIG. 8. Hugoniot diagram for the simulations of the bcc crystal. The axes are scaled with the velocities of sound. The lines serve as a guide to the eye only. The two parallel branches indicate the beginning and end of the phase transformation.

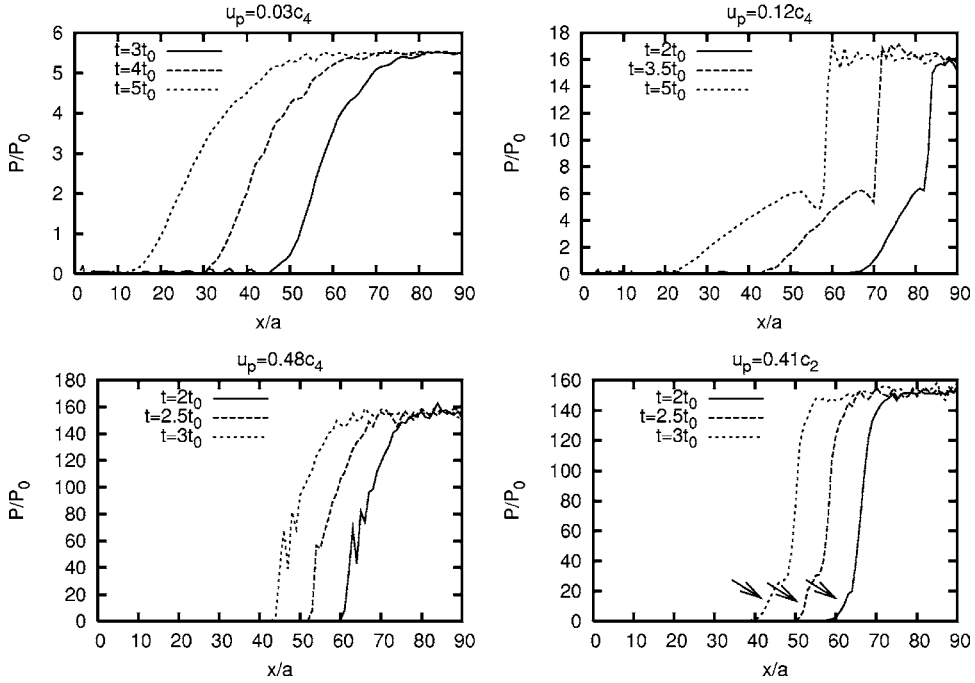

FIG. 9. Wave profiles of hydrostatic pressure in the elastic, elastic-plastic, and overdriven range. The first three plots are for the fourfold direction, the lower-right plot is for a twofold direction. The profiles in the elastic and the elastic-plastic regime (upper part) look similar for all shock wave directions and initial phases. The arrows in the lower-left part indicate the additional wave observed, for example, for bcc shocked along a twofold direction.

Above $u_p=0.2-0.25c_x$ the velocities of both waves approach each other. This part will be called the overdriven range. If the transition is sharp, as in the case of bcc shocked along the fourfold direction, a distinction between both waves no longer exists. In the other cases, especially for bcc shocked in the threefold or the twofold directions two "transformation" wave fronts are plotted. A first one that indicates that the initial phase starts to be destroyed and a high-defect phase is formed, and a second one that indicates the transition to a low-defect close-packed phase. The situation plotted in Fig. 8 is typical for short samples. If $u_p=0.3c_x$, for example, both transformation fronts have reached the same velocity after a distance of about $70a$ and the whole wave profile has become steady. If $u_p=0.5c_x$ the distance has fallen to $50a$.

Figure 9 displays some representative hydrostatic pressure wave profiles from all three ranges. In the upper part of the figure it is found that the pressure rises continuously in the elastically deformed part and that this part widens as time goes on. The plastic front, on the other hand, rises sharply and reaches a steady state. In the lower part of the figure a comparison is given between the wave profiles in the overdriven range in the fourfold direction where a direct transition occurs and the twofold and threefold directions where the bcc structure is first destroyed and a close-packed phase is formed subsequently. This double structure corresponds to the starting and ending of the phase transition as indicated in Figs. 7 and 8.

In conclusion, in the monatomic system a clear distinction exists between an underdriven elastic-plastic regime and an overdriven phase transformation regime for all cases studied, in contrast to the smooth transition that has been observed in the simulations of diatomic materials.[6]

In some cases, especially for shock waves along the threefold axis in bcc, additional phenomena are observed which will be discussed in detail in paper II. In the elastic-plastic range, a metastable phase is formed that is related to solitary waves observed in the overdriven range. These effects lead to additional wave fronts and wave velocities u and may complicate the analysis of the results. For simplicity, in Fig. 8 the wave crests related to the metastable phase and the solitary wave trains are omitted.

C. Description of the structural results

Since a lot of structures and orientations have been studied to get a general overview of the possible mechanisms, it is not possible to deal with all the cases in detail and to describe the results in dependence of the piston velocity u_p. Instead we will concentrate on a few representative cases, describe them in detail—especially the dependence on u_p—and add remarks about other structures and orientations where appropriate. We will concentrate on the elastic-plastic range, since in the elastic range no defects are created and in the overdriven range the energy stored in the structure is so high that no low-defect crystals are created during simulation.

1. The fourfold direction

The phase transition from bcc to close-packed phases for shock waves along the fourfold direction is very special. It is the only case where a perfect crystal is found after the transition and an atomically flat interface between bcc and fcc or hcp is observed. Consequently the pressure profile is steady and shows a sharp jump at the interface between bcc and the close-packed phase.

As an example, we present the results for $u_p/c_4=0.24$ in middle range. Figure 10 shows the flat interface. The orientation of the close-packed layers is such that a threefold axis is generated parallel to the shock direction. A twofold axis is parallel to the face diagonal (Fig. 11, left). This orientation is none of the well-known martensitic bcc-fcc orientation rela-

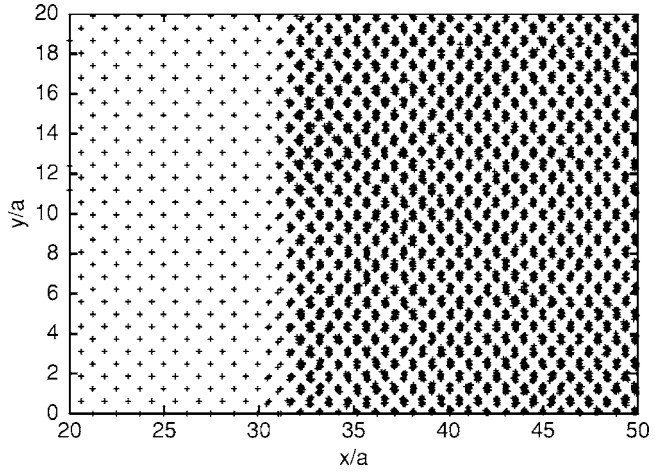

FIG. 10. Longitudinal projection of a bcc crystal shocked along the fourfold direction ($u_p=0.24c_4$). The shock wave moves to the left, the mirror is at the right side at $x=100a$. The interface between initial bcc and final fcc at about $x=31.5a$ is flat.

tionships. The stacking sequence of the layers is more or less random but sometimes rather pure fcc or hcp sequences occur. In the right part of Fig. 11, two twins are shown representing a low-energy type of defect. Due to the periodic boundary conditions there have to be two interfaces: one at $y=8a$ and one at $y=18a$. If the shock wave proceeds, the twins vanish (Fig. 11, right). The twin boundaries end at a dislocation line. We have found that the newly generated close-packed phase may change several times between twined and monocrystalline.

The transformed phase remains no longer monocrystalline when the piston velocity enters the overdriven region. Several crystallites are created, and at about $u_p=0.5c_4$, the defect density has grown so large that the sample cannot be distinguished from a disordered or an amorphous structure.

2. Other directions and structures

Shock waves along the twofold and threefold directions in bcc, in the σ phase, and the quasicrystal along any direction never lead to a direct transition to the close-packed phase. Although the statistics and the details may differ, the overall

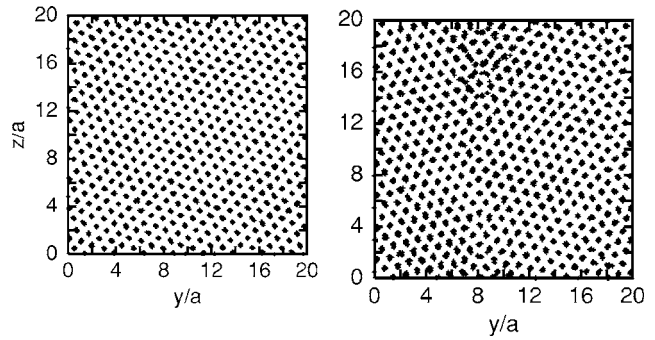

FIG. 11. Transverse cuts through a bcc crystal shocked along the fourfold direction ($u_p=0.24c_4$). The shock front is currently at $x=31a$ and moves toward $x=0$ (see Fig. 10). Left: Slice between $x=50a$ and $x=60a$, right: slice between $x=75a$ and $x=85a$.

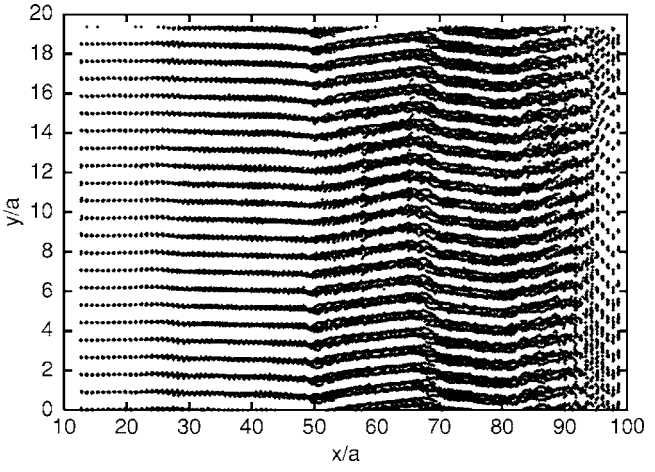

FIG. 12. Longitudinal projection of a bcc crystal shocked along the twofold direction ($u_p=0.125c_2$). This is an example where the lattice planes are shifted perpendicular to the shock wave direction. The shock wave moves to the left; the mirror is at the right side. A beginning *ABABC* stacking sequence is visible near $x/a=97$.

pattern of the phase transitions is similar. Therefore we will discuss these cases summarily.

At low shock wave intensity the general picture is that the initial structure is heavily distorted or destroyed by the arriving shock front and, at the same time, structure transformation into the close-packed phase starts.

Two cases can often be distinguished but are usually mixed up: transverse shifts that appear as a bending of the atomic layers (Fig. 12), and more complicated deformations where atomic layers are rotated around an axis parallel to the shock direction in addition to the shifts (Fig. 13). It is remarkable that there are only kinks in the atomic chains parallel to the shock wave direction, but no disruption. Few pointlike defects occur at low shock wave intensities. The whole motion of the atoms seems to be well correlated.

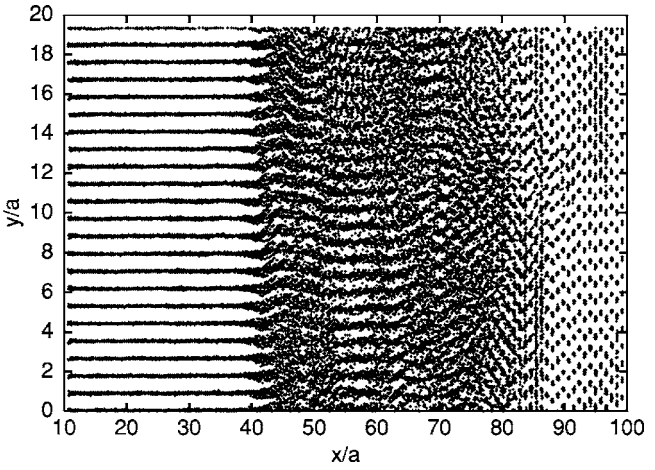

FIG. 13. Longitudinal projection of a bcc crystal shocked along the threefold direction ($u_p=0.19c_3$). This is an example where the lattice planes are rotated perpendicular to the shock wave direction. The shock wave moves to the left; the mirror is at the right side. A beginning *ABABABABABCBCAB* stacking sequence is visible between $x/a=87$ and $x/a=100$.

TABLE III. Summary of the phase transition phenomena observed at low shock wave intensity.

Structure and Orientation	Phase Transformation Phenomena
bcc fourfold	Direct transition, interface atomically flat
bcc twofold and threefold	Transverse bending and kinks, shifting or rotation of atomic layers perpendicular to shock wave direction
σ phase 0 and quasicrystal 0	Periodic modulation along the shock wave direction
σ phase $m45$ and $m90$	No special phenomena
quasicrystal 90	No special phenomena
σ phase $n90$	Periodic bands at 45° with respect to the shock wave direction
σ phase $n45$	First: transient state generated by homogeneous shear, later: kinks and bends

The final state of material is a close-packed phase with clearly defined layers perpendicular to the shock direction, but with several crystallites in the plane. Compared to the bcc case shocked along the fourfold direction, the close-packed crystal has no preferred orientation with respect to the coordinate axes, and it contains many defects and extended disorder. The details of the phase transformation differ for the different structures and orientations. Although the details might be interesting for the study of possible plasticity modes, we have collected only the most important cases in Table III.

At the end of the sample, close to the mirror, an almost perfect close-packed crystal is generated (Figs. 12 and 13). This part is clearly induced by the mirror that enforces a layering parallel to the mirror. It is not present if the collision method is used. Thus it can be regarded as an artifact. The close-packed phase itself, however, is not a consequence of the simulation method. First of all, the close-packed phase is also created in simulations with the collision method, and second, the close-packed phase is also present in the other parts of the sample as discussed before, but polycrystalline with random orientations of the crystallites and with defects.

The effect of higher piston velocity u_p is similar to the case of shock waves along the fourfold direction of bcc: the close-packed phase become polycrystalline, more and more defects are created, and if u_p reaches around 0.37 to $0.5c_x$, the structure can no longer be distinguished from an amorphous material.

3. Flipped configurations in the TCP phases

A phenomenon that is called "phason flip" in quasicrystals occurs in the tcp structures shocked along a direction that lies in the basic layer. For simplicity, the phason flips can be regarded as tile rearrangements and replacements that are possible in many nontrivial tilings.

Figure 14 shows an example of new rhombi and rearranged tiles in the σ phase shocked in $m90$ orientation. The orientations of the tiles are always the same, others are not possible for geometric reasons. In samples shocked in the $n90$ orientation the rhombi are oriented with their long diagonal parallel to the coordinate axis. In the quasicrystal both orientations are observed. The threefold symmetric hexagon has also been seen in some occasions, but the twofold symmetric hexagon never shows up, because it is very unstable. The atomic rearrangements of a flip have been described in detail by Roth.[19] All the atoms along a row perpendicular to the shock direction change from a one-dimensional configuration of atoms in the basic layer represented by a dotted ring in Figs. 1–3 to a staggered configuration represented by a open and nearby close circle or vice versa. The tiles themselves are abstract objects that have no physical meaning. Therefore it is not surprising that flips from one-dimensional to the staggered configuration are observed that lead to nontilable regions.

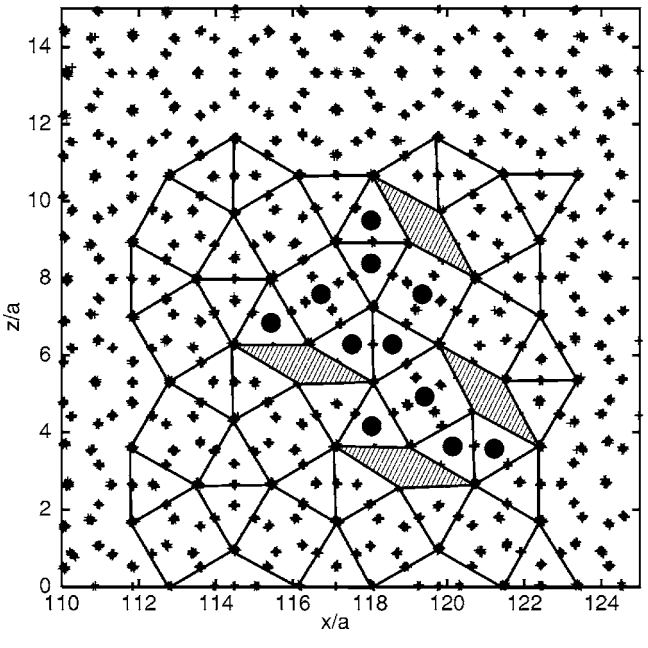

FIG. 14. Part of a σ phase sample shocked in $m90$ orientation, $u_p=0.125c_x$. A part of the tiling has been redrawn. Shaded are the newly generated rhombi. The black dots mark the squares and triangles that have been flipped. The shock wave moved from the right to the left.

4. Special phenomena for shock waves along the threefold direction of bcc

If shock waves are studied in bcc along the threefold direction, an intermediate phase and wave phenomena are observed, which are denoted "solitary waves" since they show up as singular, roughly Gaussian shaped dispersionless maxima. We think that this name is appropriate although the solitary waves decay slowly. But since we have not demonstrated the collision property, we will not call the peaks solitons. The intermediate phase has been identified as the hexagonal two-layer ω phase.[16] It is the crystal structure of AlB_2 and ω-CrTi, and occurs in the phase diagram of the elements Ti, Zr, and Hf. The ω phase is also well known as a consequence of phonon softening along the threefold direction in bcc. The ω phase and the solitary waves are closely related and will be presented in detail in Paper II.

5. Results for an amorphous structure

Shock waves have been studied in an amorphous structure produced by cooling a molten bcc crystal. Since there is no liquid phase for the Dzugutov potential at ambient pressures,[13] we had to prepare the liquid by heating at constant volume, cool it down to $kT=0$, and expand it to $P=0$.

The amorphous structure generated from the liquid has a RDF that differs from an ordinary monoatomic amorphous structure generated with Lennard-Jones potentials for example. The difference is caused by the outer maximum of the Dzugutov potential. The RDF shows the well-known behavior of a super-cooled liquid with a first maximum for nearest neighbors and a double maximum for next-nearest neighbors, but the first of the two next-nearest-neighbor peaks is extremely sharp if compared with what is usually observed. The third maximum seems to be enhanced also. See Fig. 16 where the curve for $u_p=1.0v_0$ is more or less identical with the unshocked state. The stress-temperature curves for the shocked state have been included in the equilibrium phase diagram (Fig. 4). The curves are somewhat lower than those for the initially ordered structures. The most important difference, however, is the observation that for the amorphous structure, the temperature of the shocked state is always well defined.

The Hugoniot curve (Fig. 15) shows that at low piston velocities the velocity of the wave front at half height is almost constant. The distance between the bottom (amo_b) and the place where the wave reaches a constant value grows and the difference is most prominent around $u_p/c_a<0.1$. If the piston velocity is increased the ascent of the wave gets sharper and sharper until the difference between the velocities vanishes in the overdriven regime. The width of the transition region is of the order 5 to 10 atom distances a.

In the RDF we find a rather sharp transition at the beginning of the overdriven regime at about $u_p/c_a<0.4$ (Fig. 16). At low piston velocities, the first maximum of the RDF lies around $1.05a$, then it moves to $0.85a$ and broadens slightly. The most significant change occurs to the sharp subpeak of the second maximum: It stays at its place, but broadens from a width of $0.1a$ to $0.5a$. The other subpeak vanishes completely and the third maximum moves by $0.3a$ and doubles its width. At the highest piston velocities the RDF looks like one of an ordinary monatomic liquid.

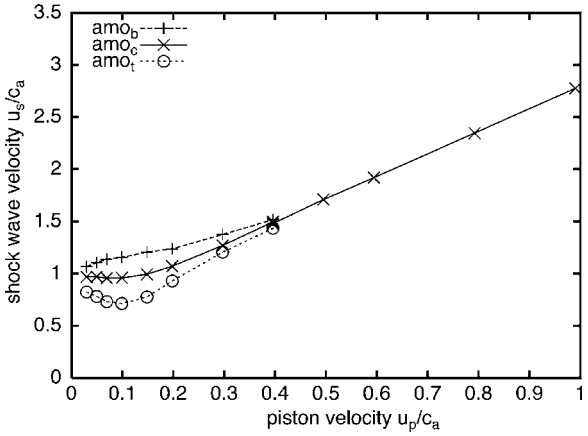

FIG. 15. Hugoniot curve u_s vs u_p for the amorphous structure. Plotted are the velocities at the bottom (amo_b), at half height (amo_c), and at the place where the hydrostatic pressure reaches a maximum (amo_t). In the overdriven region, the distinction between these velocities vanishes, which means that we find a sharp wave front.

The ADF possesses two broad maxima at an angle of 60° and at 112°. In the shocked samples these maxima shift continuously to 57° and 110°, respectively, if the piston velocity is increased.

The sharp transition indicates that the behavior of the material changes from glasslike to liquidlike if the piston velocity increases from weak shocks to overdriven shocks. The kinetic energy of the atoms is high enough that the repulsive outer maximum of the Dzugutov potential no longer plays a role at the high piston velocities.

In contrast to all other samples studied in this paper no transition to fcc is observed. This is already obvious from the RDF since no maximum or shoulder exists around the distances $1.25a$ and $1.55a$. The ADF has no maxima at 90°, 150°, and 180°. All together this proves that there are no square arrangements of atoms and no nuclei of a close-packed phase. A modulation of the density occurs only closely to the momentum mirror.

Compared to the shock waves in the ordered structures we find no crystallization. This indicates that it is easier to shift

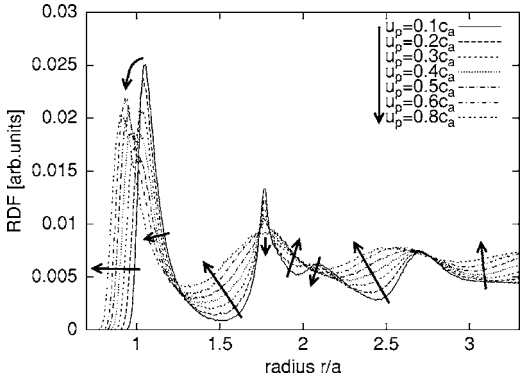

FIG. 16. RDF of the amorphous sample for different u_p. The arrows indicate how the RDF changes if the shock strength is increased from $u_p=0.1c_a$ to $u_p=0.8c_a$ ($c_a\approx 10v_0$).

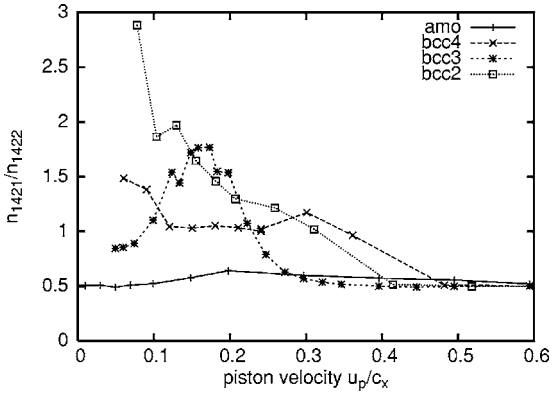

FIG. 17. Relative frequency of the 1421 and 1422 common neighbor diagrams for some representative cases.

atomic layers collectively to generate a new structure than to crystallize an amorphous material.

D. Common-neighbor analysis

The common-neighbor analysis has been carried out for all structures and orientations investigated in the preceeding sections. Here we will present only a representative selection. For the amorphous structure the fraction n_{1421}/n_{1422} is always close to 0.5 (Fig. 17), which indicates complete disorder (compare to Honeycutt and Anderson[22]) and no crystallization. Therefore the distinction between fcc and hcp is difficult. We know, however, that a bcc crystal shocked along the fourfold direction with $u_p=0.24c_4$ results in nearly perfect hcp (compare to Fig. 10), and this structure has $n_{1421}/n_{1422}\approx 1$. Furthermore, perfect fcc should yield $n_{1421}/n_{1422}\rightarrow\infty$. Thus the higher values of n_{1421}/n_{1422} clearly indicate fcc stacking. On the other hand, it is obvious that disorder grows with increasing piston velocity.

From the diagram we read off three cases in addition the amorphous case. bcc shocked along the twofold axis prefers fcc stacking at low piston velocities. The σ phase shock in the $m45$ direction behaves similarly. bcc shocked along the threefold direction behaves differently: it is hcp at low piston velocities and becomes preferably fcc stacked around $u_p/c_3 \approx 0.15$. bcc shocked along the fourfold direction is always preferably hcp stacked. The quasicrystal shocked along the $m90$ direction is similar. The other structures, the σ phase shocked along the $n45, m90$, and 0 direction; the quasicrystal shocked along the 0 direction; and the σ phase along the $n90$ direction lie between bcc shocked along the threefold and the fourfold direction, in the given ordering. The fluctuations of n_{1421}/n_{1422} are large if the results for neighboring piston velocities are compared. The data should be regarded with some care especially for low piston velocities since the new phase forms rather slowly. For example, the point at $u_p=0.8c_2$, $n_{1421}/n_{1422}=2.9$ may be too high. But if subsequent snapshots of the simulations are compared it is found that n_{1421}/n_{1422} varies rather smoothly. Usually the results do not depend strongly on the size of the sample, but for the σ phase shocked along the $n45$ and $m45$ it has been observed that special transition modes lead to a strong preference of hcp stacking.

IV. DISCUSSION

A. Comparison to shock wave simulations of iron

Kadau *et al.* have carried out molecular dynamics simulations of bcc iron single crystals.[5,25,26] Instead of a simple pair potential they used EAM potentials especially adjusted to the properties of iron. Despite these differences their results and ours are in good qualitative agreement. There are several reasons for this observation: The phase diagram of iron[27] and for the Dzugutov potential[9] is similar, i.e., both possess at low temperatures a low pressure bcc and a high pressure close-packed phase. Furthermore, if the elastic constants are computed for the Dzugutov potential and compared with the relative values c_{11}/c_{44} and c_{12}/c_{44} for iron[28] it is found that these values are closer in the diagrams (Fig. 2 of Every[28]) than to any other material.

Due to the similarity of the phase diagram, the Hugoniot for iron (Kadau *et al.*,[25] Fig. 4) and bcc with Dzugutov potentials (Fig. 8) is qualitatively similar. The results for the fourfold direction are also in good agreement, however we did not observe the compressed bcc inclusions [Kadau *et al.*,[5] Fig. 1(b)]. It is possible that they have been missed since their u_p interval of occurrence is rather small.

Twinning is also prominent in our simulations (Fig. 11), and the growth of the crystallites with time (Kadau *et al.*[26]) has also been noticed. Another important coincidence[15] is the solitary waves that occur for both interactions along the same threefold direction. They will be discussed in detail in paper II.

There are also some notable differences. The figures of structures generated by shock waves along the twofold and threefold axis[25] look similar at a first glance. Kadau *et al.* only remark that the grains in these situations are smaller than for the fourfold case. Furthermore a broad range of elastically compressed material is seen. The mechanism of phase transformation seems to be similar to the fourfold direction. But if we take our Figs. 12 and 13 into account, we find a correlated transverse motion of lattice planes, i.e., a martensitic type of transformation.[30] The ω phase has not been reported for EAM iron. At last we want to remark that there is a difference in the final structures. The EAM potential clearly favors a hcp phase (Kadau *et al.*,[25] Fig. 3), whereas we get a mixture of stackings of the close-packed layers. The reason for this difference is not obvious since the range of the EAM potential is similar to the range of the Dzugutov potential. We attribute the different behavior to the many-body part of EAM that is lacking for the pair potential. Therefore, there is no difference in energy for *ABA* or *ABC* stacking for the Dzugutov potential whereas the EAM potential favors fcc *ABC*.

B. Conclusions

We have presented detailed studies of shock waves in several structures that are stabilized by the Dzugutov potential. There are at least three major results. The Dzugutov potential which has been designed for a completely different purpose is suitable to study qualitative features of bcc metals, such as iron. It may even be possible to get to a semiquantitative or quantitative agreement if the Dzugutov poten-

tial is modified by fitting it directly to the iron properties. A second major result is the generation of special defects in the tcp phases, which are equivalent to the phason flips in quasicrystals. This effect has been observed now on several occasions, here and in binary quasicrystals.[7] Since the defects occur especially in the uniaxially compressed part of the sample it also represents evidence of the coupling between phononic and phasonic degrees of freedom[29] of a quasicrystal. In the end this means that although we have not (yet) found evidence for extended defects like phason walls generated by shock waves, we have observed the creation of point defects and phason-type flips. Furthermore we have presented simulations of a Dzugutov glass and found that no crystallization occurs that tells us that the pre-existing bcc or tcp order helps the structures in the phase transition and shows that the transition is a correlated phenomenon.

ACKNOWLEDGMENTS

I am especially indebted to H.-R. Trebin and Christoph Rudhart for many helpful discussions. The collaboration with Kai Kadau from Los Alamos National Lab and the hospitality there is also gratefully acknowledged. Franz Gähler supplied the data for the quasicrystal model.

[1] T. C. Germann, B. L. Holian, P. S. Lomdahl, and R. Ravelo, Phys. Rev. Lett. **84**, 5351 (2000).
[2] S. Zybin, V. V. Zhakhovskiĭ, M. L. Elert, and C. T. White, *AIP Conf. Proc.*, Portland, Oregon, Vol. 706, edited by M. D. Furnish, Y. M. Gupta, and J. W. Forbes (AIP, New York, 2004), p. 310.
[3] B. L. Holian, in *High-Pressure Shock Compression of Solids VI*, edited by Y. Horie, L. Davison, and N. N. Thadhani (Springer, New York, 2002), p. 149.
[4] D. Tanguy, M. Mareschal, P. S. Lomdahl, T. C. Germann, B. L. Holian, and R. Ravelo, Phys. Rev. B **68**, 144111 (2003).
[5] K. Kadau, T. C. Germann, P. S. Lomdahl, and B. L. Holian, Science **296**, 1681 (2002).
[6] J. Q. Guo, E. Abe, and A. P. Tsai, Phys. Rev. B **62**, R14605 (2000).
[7] J. Roth, Phys. Rev. B **71**, 064102 (2005).
[8] C. L. Henley, Phys. Rev. B **34**, 797 (1986).
[9] J. Roth, Ph.D. thesis, Universität Stuttgart, 1992.
[10] C. Dilger, R. Mikulla, J. Roth, and H.-R. Trebin, Philos. Mag. A **75**, 425 (1997).
[11] E. Cockayne and M. Mihalkovič, Philos. Mag. Lett. **79**, 441 (1999).
[12] J. Roth and A. R. Denton, Phys. Rev. E **61**, 6845 (2000).
[13] J. Roth, Eur. Phys. J. B **14**, 449 (2000).
[14] M. Dzugutov, Phys. Rev. Lett. **70**, 2924 (1993).
[15] J. Roth, following paper, Phys. Rev. B **72**, 014126 (2005).
[16] C. M. Wayman and H. K. D. H. Bhadeshia, in *Physical Metallurgy* Vol. II, edited by R. W. Cahn and P. Haasen (North Holland, Amsterdam, 1996), p. 1546.
[17] M. Dzugutov, Phys. Rev. A **46**, R2984 (1992).
[18] J. Roth (unpublished).
[19] J. Roth and F. Gähler, Eur. Phys. J. B **6**, 425 (1998).
[20] M. Deza and M. Shtogrin, Discrete Math. **244**, 43 (2002).
[21] B. L. Holian and P. S. Lomdahl, Science **280**, 2085 (1998).
[22] J. D. Honeycutt and H. C. Andersen, J. Phys. Chem. **91**, 4950 (1987).
[23] A. S. Clarke and H. Jónsson, Phys. Rev. E **47**, 3975 (1993).
[24] J. Stadler, R. Mikulla, and H.-R. Trebin, Int. J. Mod. Phys. C **8**, 1131 (1997);J. Roth, F. Gähler, and H.-R. Trebin, Int. J. Mod. Phys. C **11**, 317 (1997).The home page of *IMD* can be found at www.itap.physik.uni-stuttgart.de/~imd
[25] K. Kadau, T. C. Germann, P. S. Lomdahl, B. L. Holian, and F. J. Cherne, *Proceedings of the 13th American Physical Society Topical Conference on Shock Compression of Condensed Matter*, edited by M. D. Furnish, Y. M. Gupta, and J. W. Forbes, AIP Conf. Proc., Portland, Oregon, Vol. 706, (AIP, New York), p. 229.
[26] K. Kadau, Ph.D. thesis, Universität Duisburg, 2001.
[27] J. C. Boettger and D. C. Wallace, Phys. Rev. B **55**, 2840 (1997).
[28] A. G. Every, Phys. Rev. B **24**, 3456 (1981).
[29] U. Koschella, F. Gähler, J. Roth, and H.-R. Trebin, J. Alloys Compd. **342**, 287 (2002).
[30] In the interpretation of these results one has to be very careful if, for example, the coordination number is taken as an indication of the structure or defects since the material is compressed uniaxially and the ideal coordination numbers are no longer valid. If a radial criterion is used, we find that a shift of the cutoff radius by less than a percent can change the picture completely since the atom shells of bcc and of the close-packed phase are rather broad and overlap partially which may mimic the presence of point defects (see Ref. 25, Fig. 2).